Taming Oxygen in the Electron Microscope

Effects of High Energy Electron Irradiation on O_2 and Oxides

DAVID WAHLQVIST
DEPARTMENT OF CHEMISTRY | FACULTY OF ENGINEERING | LUND UNIVERSITY
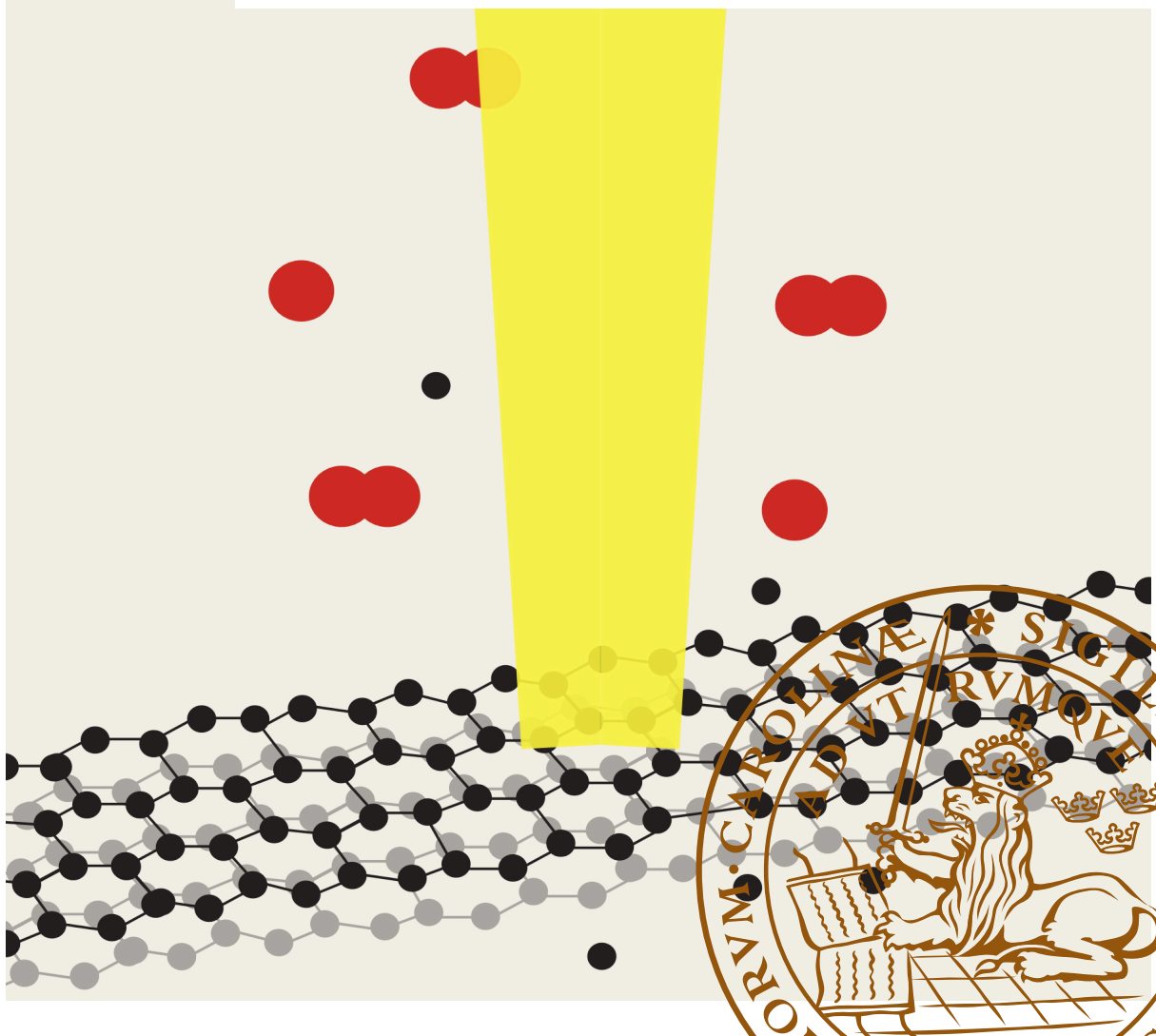
Taming Oxygen in the Electron Microscope

Taming Oxygen in the Electron Microscope

Effects of High Energy Electron Irradiation on O_2 and Oxides

by David Wahlqvist

LUND
UNIVERSITY

Thesis for the degree of Licentiate
Thesis advisors: Martin Ek Rosén
Faculty opponent: Dr. Sebastian Pirel Jespersen

Abstract

Transmission electron microscopy (TEM) is an atomic resolution technique that allows for in depth analysis of the properties of different materials by passing high energy electrons through a thin sample and detecting how they are affected. However, due to the strong interaction between electrons and matter, the probability of the sample remaining unperturbed by the electron irradiation is small. This is an issue as there can be ambiguity about if the effects seen in TEM are inherent for the material or induced, fully or in part, by electron irradiation.

One especially useful application of TEM is to observe dynamic processed by introducing external stimuli such the introduction of reactive gases into close proximity of the sample, referred to as Environmental TEM (ETEM). ETEM allows for the observation of morphological, elemental, atomic, and chemical changes in a solid in a solid–gas reaction, providing insight into the function of the solid during the reaction. However, during dynamic processes, due to the increased complexity of the interactions, it is even more difficult to deconvolve the inherent effects from the ones induced by electron irradiation. When a reactive gas is introduced into the TEM, it will be affected by the electron irradiation and may become even more reactive. The gas may also interact with defects in the sample caused by electron irradiation. Both these interactions generally lack equivalents in applications outside the ETEM, resulting in further ambiguity.

Herein I discuss the ramifications of electron irradiation in TEM, both in vacuum and with reactive gases present, especially as they pertain to carbon black oxidation and the electron irradiation induced oxidation of cobalt nickel nanoparticles. In both of these cases there is a substantial effect from electron irradiation. For carbon black oxidation, the oxidation rate is highly dependent on the electron flux and in observations of cobalt nickel nanoparticles, electron irradiation induces surface oxidation of the particles. In this thesis I provide some suggestions for how the interpretative problems arising from electron irradiation can be compensated for, and how to best mitigate the effects in the first place.

DOKUMENTDATABLAD enl SIS 61 41 21

Taming Oxygen in the Electron Microscope

Effects of High Energy Electron Irradiation on O_2 and Oxides

by David Wahlqvist

LUND UNIVERSITY

A licentiate thesis at a university in Sweden takes either the form of a single, cohesive research study (monograph) or a summary of research papers (compilation thesis), which the licentiate student has written alone or together with one or several other author(s).

In the latter case the thesis consists of two parts. An introductory text puts the research work into context and summarizes the main points of the papers. Then, the research publications themselves are reproduced, together with a description of the individual contributions of the authors. The research papers may either have been already published or are manuscripts at various stages (in press, submitted, or in draft).

"Um, no one reads the [Theses], Insert Name Here. They appear to be what we in the trade call write-only documents." – Terry Pratchett

… I don't think it was for reading. It was for having written…" – Terry Pratchett

Contents

List of publications

This Licentiate thesis is based on the following publications and data surrounding them, referred to by their Roman numerals:

I   **Impact of electron beam irradiation on Carbon Black oxidation in the ETEM**

    D. Wahlqvist, M. Mases, D. Jacobsson, H. Wiinikka, M. Ek.
    Manuscript in preparation, unpublished

II   **Effect of the carrier gas on the structure and composition of Co–Ni bimetallic nanoparticles generated by spark ablation**
    P. Ternero, M. Sedrpooshan, **D. Wahlqvist**, B.O. Meuller, M. Ek, J.M. Hübner, R. Westerström, and M.E. Messing.
    Journal of Aerosol Science, 2023, 170, pp. 106146

Paper I is a manuscript and published as is. Paper II is reproduced under the Creative Commons CC–BY license.

Acknowledgements

A lot of work goes into this type of thesis, and as such there are quite a few people involved behind the scenes. As such, there are a couple of people I want to thank for help in creating this Licentiate thesis.

Firstly, I would like to thank my supervisor, Martin Ek, who has been very helpful in providing insight into the science involved with the content of this thesis. Martin has supplied me with much feedback and many fruitful discussions about the interpretation of data and the conclusions drawn from it. Thank you for taking so much time to aid me in becoming a better researcher, I hope that you will see the results of your work in the next two years.

I would also like to acknowledge the contributions of my proofreaders, Microsoft Word spellcheck has been a lifesaver, no but really, Miķelis, Robin, Tianyi, and again, Martin. Thank you for your insightful comments on the content, language usage, spelling, inappropriate use of archaic words or grammar and general comments. I find long convoluted sentences fun to write, but can agree that they are not very enjoyable to read.

What would a Kappa be without the papers to go along with it? Well, 47 pages shorter for a start. But also essentially non–existent, so therefore I would like to thank my collaborators on the papers presented herein for their valuable contributions.

Penultimately (again with somewhat archaic word usage), I would like to thank my family for their support and pestering about how the writing is going. However, my sister Elin deserves specific mention, not only for the cover image, which is a magnificent job considering the, frankly terribly unclear, sketch that I gave to her. But also for taking care of our shared apartment for these last couple of weeks when I have spent an inordinate time writing and not doing my fair share of the housework.

And finally, I would like to dedicate (on her insistence) Table 1 to my wonderful girlfriend Malin, who has supported me through this somewhat stressful time.

Populärvetenskaplig sammanfattning på svenska

Att undersöka materialegenskaper på atomnivå är något som kan ge en enorm insikt i hur material beter sig fundamentalt. Ett viktigt verktyg som tillåter undersökning av just detta är ett så kallat transmissionselektronmikroskop (TEM), där elektroner får passera genom ett prov och sedan analyseras. En jämförelse kan göras med ett vanligt ljusmikroskop där ljus får färdas igenom ett prov så att det skapas en virtuell bild av provet, bilden utav provet blir förstorad med hjälp av olika glaslinser, och denna förstorade bild får nå våra ögon. I TEM så passerar elektroner genom ett prov, interagerar med provet så att det skapas en virtuell bild, bilden förstoras med hjälp av elektromagnetiska linser, och detekteras sedan av en specialbyggd detektor som kan mäta elektroner. Den stora skillnaden mellan just ljusmikroskopi och elektronmikroskopi är att elektroner interagerar mycket mer med materia än vad ljus gör. Detta leder till att provet vi kollar på i TEM är starkt påverkat av att vi kollar på det. Då kommer frågan upp om det vi ser i TEM är representativt av vad som verkligen är där.

Denna fråga försvåras ännu mer när vi värmer provet, eller utsätter det för gaser, eller på annat sätt påverkar provet externt för att se vad som händer då. Här är det värt att notera att vanligt TEM sker i vakuum då den starka interaktionen mellan elektroner och material, såsom en gas, är såpass stor att den påverkar bruset i datan märkbart, det kan till och med vara så att inga elektroner når detektorn. När vi tillför gas till ett TEM system så kallar vi det för Environmental TEM eller ETEM. I ETEM finns det mer än bara provet vi kollar på som elektronerna kan interagera med, de kan interagera med gasen också. Denna extra påverkan från gasen möjliggör en massa fler interaktioner då gasen generellt kommer bli mer reaktiv efter att ha exponeras för elektroner med hög energi. Dessutom så kan elektronerna, precis som i TEM, skada provet, och dessa skador kan vara mer känsliga för gas och reagera snabbare eller på ett annat sätt än vad som hade skett om inte en massa elektroner interagerar med provet.

Således är det väldigt viktigt att förstå sig på precis hur elektronerna påverkar systemet, det vill säga provet och gasen. Vi måste veta om det vi ser är något fundementalt för provet eller om det är någonting som elektronerna inducerar eller på annat sätt påverkar. Tar vi inte reda på detta är det enkelt att dra felaktiga slutsatser kring det vi ser i TEM och ETEM.

Part I

Research Context

Chapter 1: Introduction

Transmission electron microscopy (TEM) has proved to be a useful instrument primarily in material science and biology as it facilitates the acquisition of atomic resolution data of materials. Additionally, this atomic resolution can be combined with various spectroscopic methods providing both chemical and elemental composition. Because of these properties, TEM has provided great insight into the atomic nature of many different materials [1, 2]. It also fills a niche as a routine analysis instrument, and has been used for crystallographic analysis of nanoparticles [3, 4] or for the collection of data used in 3D–reconstruction of biological specimens, primarily viruses and proteins [5, 6, 7], among many others. However, there is potential for a question relating to the reliability of the results. The sample is necessarily exposed to a constant, high magnitude flux of high energy electrons in order to acquire micrographs with a good signal–to–noise ratio. These electrons carry a large amount of energy, some of which is they can transfer to the sample. This results in a sample that is highly perturbed during observation, which raises the question of which phenomena observed in the electron microscope are inherent to the sample, and which are affected by the necessary presence of high energy electron irradiation.

Electron beam effects therefore requires careful consideration in any study involving electron microscopy due to the profound impact they have on materials. Effects from electron irradiation have therefore been studied extensively for a myriad of materials, such as oxides [8, 9], carbon nanostructures [10], organic thin films [11], and metals [12], as well as receiving copious theoretical treatment [13]. However, there are still unexplored avenues of the effect as characterization of the effects are lacking in certain cases, and there is some debate on the exact mechanisms behind some of the more complex particularities of this important effect.

This thesis consists of two parts, the first part aims to provide a background and theory as to put my contributions to the scientific field in context. The remainder of the Chapter 1 deals with a brief introduction into the Transmission electron microscope and the environmental transmission electron microscope. Chapter 2 discusses how the electrons used

to probe the sample can interact with the sample to change the sample during observation, and provides a theoretical framework for electron interactions with matter. Chapter 3 discusses further details of the electron beam effects as they pertain to electron–gas interactions and electron–gas–solid interactions. Chapter 4 discusses potential mitigation techniques, both in the case without gas present, and additional opportunities that arise when introducing gas into the electron microscope. Finally, Chapter 5 summarizes the findings and discusses future avenues of exploration.

1 Transmission electron microscope

To begin a discussion regarding how electron irradiation affects different materials during static and dynamic processes in the transmission electron microscope (TEM[1]), it is pertinent to include a short introduction into the function and usage of the TEM. In the most basic of terms, to conduct TEM characterization, three components are required, a sample, an electron source, and a detector. These three components are connected with different lenses, and several detectors are present, however, they are not vital to the discussion, and will therefore not be discussed. What is important for this discussion is that high energy electrons pass through a sample and are detected by a detector. For a more detailed dive into the actual mechanics of the TEM, recommended references are references [14, 15] additionally, for a more historical contemplation with beautiful images acquired on film, there is also reference [16].

In a bit more detail, the important mechanics are: electrons are emitted from the electron source and are accelerated to high energies, generally between 80 keV and 300 keV. These electrons pass through a sample, with which they interact, the nature and magnitude of the interaction dependent on the material in question as well as on the energy of the incoming electrons. Following the interaction, the results detected by a detector. The detection can be of high energy electrons, having been scattered by the sample to provide spatial information; or having lost energy through various interactions and providing chemical and elemental information. The detection can also be of secondary effects resultant from the interactions from electrons passing through the sample. These secondary effects can be characteristic X-rays or secondary electrons emitted from the sample, which carry elemental and surface information respectively.

While these questions are important for static TEM observations, especially for those relating to biological material, they are even more important when the sample is probed in some way, i.e. in dynamic processes. The prime example of this is Environmental TEM (ETEM), where gases are introduced into the area surrounding the sample.

---

[1]Do note that TEM is both used to describe the instrument, as in transmission electron microscope, but also the act of using the instrument, as in transmission electron microscopy.

1.1 Environmental transmission electron microscopy

ETEM is a development of TEM wherein gases are injected into the microscope near the sample in order to observe dynamic processes as the sample interacts with the gas. However, due to the proclivity of electrons to interact with matter, electron microscopy attains optimum resolution at low pressures, i.e. less interactions with a gas results in more electrons reaching the detector. Optimally, an electron in the microscope would interact only with the sample, and as such if there are gas molecules present, they will contribute to loss of resolution through a variety of factors, including energy loss of some of the electrons resulting in their focusing by the lenses changing. Additionally, some components of the microscope, notably the electron source, must remain under high vacuum to function at all. This puts some pressure on the design of an ETEM. There must be apertures and copious pumping capacity to restrict gas flow to places in the microscope where there should be a relative vacuum. In order to attain atomic resolution, there should be compensation for the resolution loss caused by the introduction of gas into the column. For further information regarding the two ETEMs, reference [17] and [18] provide more details regarding their respective ETEMs.

Despite the operational difficulties, the possibility of observing materials during exposure to gases is an important tool for understanding dynamic processes such as oxidation [19, 20], reduction [21, 22, 23], and crystal growth[24, 25]. For these applications, ETEM is an unparalleled instrument for obtaining insight into dynamic processes.

However, the introduction of gas near the sample further exacerbates the issue of electron irradiation of the sample as several additional avenues of interaction are made available. Not only can the electrons interact with the solid, they can also interact with the gas which would then react with the solid, or they can interact with the solid which the gas can react with, or indeed they can interact with gas molecules already adsorbed to the solid. These additional interaction possibilities complicate the analysis of data collected in ETEM since it is difficult to determine which observed effects can be attributed to intrinsic processes and which can be attributed to electron interaction induced, or at least influenced, processes.

Chapter 2: Theory of beam–sample interactions

Using TEM to analyze material properties is common, and provides insight into the atomic nature of the sample. However, while the material is being analyzed, it is also interacting with the high energy electrons passing through it. Therefore, in order to understand if the material is being meaningfully perturbed, electron–sample effects must be considered. To begin the discussion in a constructive way, a theoretical description of what effects the electrons can induce, and the theory behind electron–beam effects is useful.

Electron–sample interactions are commonly split into two different categories depending on whether the incoming electron interacts with the nucleus of the target atom, or its electron cloud. Interactions with the nucleus of the target atom involves an interaction between two objects of very different masses, as such the momentum transfer is small, leaving the electron with a around the same energy as it started with, therefore this interaction is referred to as elastic. Interactions with the electron cloud on the other hand involve a much larger potential transfer of momentum and are referred to as inelastic.

Within these two larger categories of elastic and inelastic beam damage, there exist a few more subdivisions. As per Egerton et al [13] inelastic effects can be subdivided into electron beam–induced heating, where energy transferred from high energy electrons mainly becomes heat resulting in an increase in temperature; and ionization of the sample, leading to emission of secondary electrons and X–ray emission as well as general charging of the sample. Furthermore, radiolysis is another inelastic effect described as general electron beam induced degradation by inelastic scattering. Elastic effects consist of atomic displacement, also called knock–on damage, wherein electrons knock atoms away from their crystallographic positions, if this occurs at a surface, atoms will be displaced into the vacuum, which is referred to sputtering. There is also electrostatic charging, whereby a net charge is accumulated in the sample, which has contributions from both elastic and inelastic effects.

1 Interaction Cross–sections

In order to describe the probability of two particles interacting, a so–called interaction cross–section is constructed. This cross–section tends to depend on the energy of the incoming electron as well as some universal constants and some material specific constants. The cross–section as a unit of probability arises from the classical view of two spheres colliding with each other, where the probability of their interaction is determined by their respective radii. A few important cross–sections pertaining to my contributions are the ionization cross–section, when inelastic interactions result in the target material gaining or losing an electron; and the sputtering cross–section, whereby an elastic interaction between the electron and the target material results in an atom of the target material being sputtered into the vacuum.

1.1 Ionization Cross–section

In order to model the ionization cross–section, which is relevant for modeling the degree of ionization within the gaseous phase of the ETEM, a so–called binary–encounter model is used. Kim et al. proposed a model they called the Binary–encounter–dipole (BED) model [26], a combination of binary–encounter theory and Bethe theory. The BED model allows for the calculation of the energy distribution of electrons ejected from an atomic or molecular orbital during interaction with an incoming electron of energy T. The BED model requires several input data; the electron binding energy (B), the average kinetic energy (U), the orbital occupation number (N), and the continuum dipole oscillator strength for each orbital. The BED model results in good approximations of the cross–sections for small atoms and molecules. However, it requires the dipole oscillator strength to be known, and while in principle, it can be calculated, it is non–trivial to do so. Therefore, if the dipole oscillator strength is assumed to be a constant some simplifications to the BED model can be made, resulting in the Binary–encounter–Bethe (BEB) model.

$$\sigma_{BEB} = \frac{S}{t+u+1} \left[\frac{\ln(t)}{2} \left(1 - \frac{1}{t^2} \right) + 1 - \frac{1}{t} - \frac{\ln(t)}{t+1} \right] \tag{1}$$

where,

$$S = \frac{4\pi a_0^2 N R^2}{B^2} \qquad u = U/B \qquad t = \begin{cases} T/B & \text{if } T/B > 1, \\ 1 & \text{if } T/B \leq 1. \end{cases}$$

Where a_0 is the Bohr radius and R is Rydberg energy. Equation 1 is referred to as the Binary–encounter–Bethe (BEB) model [27] and only requires the theoretically determined average kinetic energy and occupation number, as well as the either theoretically or experimentally determined binding energy of each atomic or molecular orbital. In order to calculate the total ionization cross-section, the sum of the BEB model for each atomic orbital is calculated.

While fairly accurate at lower electron energies ($T < 10\,000\,\text{eV}$), at higher electron energies relativistic effects need to be accounted for in order to maintain the accuracy of the model. The relativistic version of the BEB model (RBEB) [28] is again a simplification of the relativistic version of the BED model (RBED)[2]. The RBEB model is listed in Equation 2.

$$\sigma_{RBEB} = \frac{4\pi a_0^2 \alpha^4 N}{\left(\beta_t^2 + \beta_u^2 + \beta_b^2\right) 2b'} \left\{ \frac{1}{2} \left[\ln\left(\frac{\beta_t^2}{1 - \beta_t^2}\right) - \beta_t^2 - \ln(2b') \right] \left(1 - \frac{1}{t^2}\right) \right.$$
$$\left. + 1 - \frac{1}{t} - \frac{\ln(t)}{t+1}\frac{1 + 2t'}{(1 + t'/2)^2} + \frac{b'^2}{(1 + t'/2)^2}\frac{t - 1}{2} \right\} \quad (2)$$

where,

$$\beta_t^2 = 1 - \frac{1}{(1 + t')^2} \qquad\qquad t' = \frac{T}{mc^2}$$
$$\beta_u^2 = 1 - \frac{1}{(1 + u')^2} \qquad\qquad u' = \frac{U}{mc^2}$$
$$\beta_b^2 = 1 - \frac{1}{(1 + b')^2} \qquad\qquad b' = \frac{B}{mc^2}$$

Where, in addition to the definitions relating to Equation 1, α is the fine structure constant, and c is the speed of light.

The total ionization cross–section, which is useful for describing what fraction of material will be ionized at certain conditions, is calculated by summing Equation 2 over all relevant orbitals. Data for such summations can be determined experimentally or theoretically[3], an example for values for O_2 in a triplet state is found in Table 1 in Chapter 3.

Solving Equation 2 for all relevant molecular (or atomic) orbitals at many different energies gives the expected energy dependence of the ionization of the the molecule. In

---

[2]A discussion of both BED and RBED are excluded from this text for the sake of relative brevity.
[3]These are often tabulated and can, for example, be found, with sources, on NIST's website.

general, the solution will involve some threshold energy below which the ionization does not occur, after which it reaches a maximum and then declines with increasing T. This is illustrated in Figure 1.
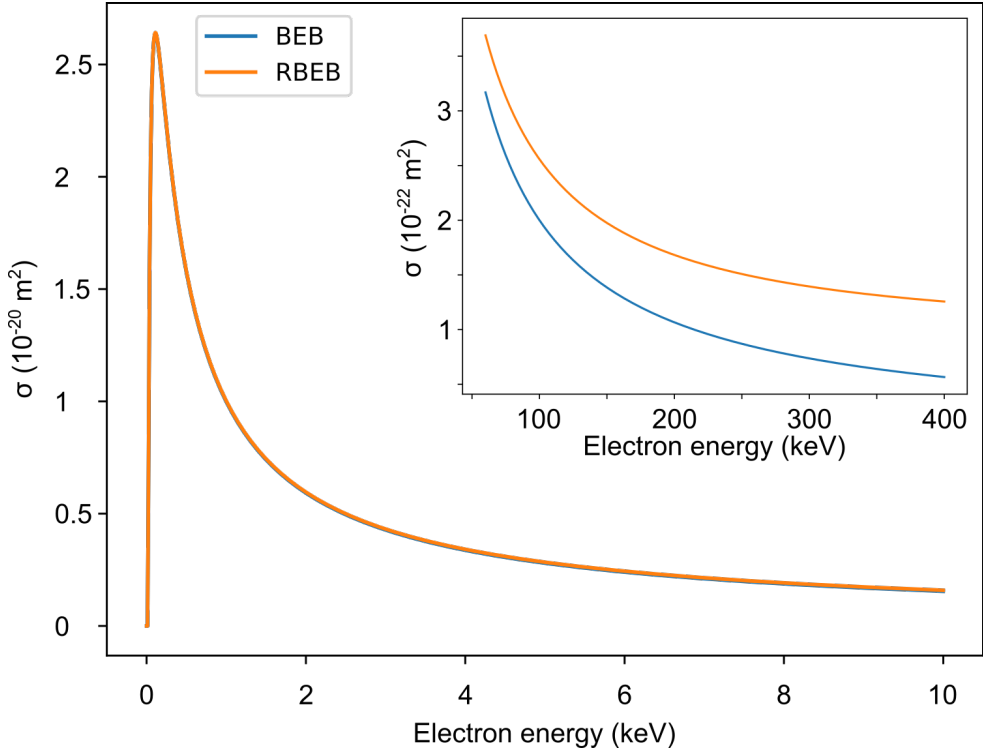
Figure 1: RBEB calculations for O$_2$ with the values found in Table 1. The inset shows how the cross–section changes at higher energies, note the two orders of magnitude smaller cross–sections than in the main figure.

1.2 Sputtering

Another important type of cross–section is the sputtering cross–section, which describes the probability of the elastic effect of knocking an atom away from its lattice position into the vacuum. This cross–section can be calculated by using the McKinley–Feschbach approximation of the Mott cross–section [29].

$$\sigma_d = \frac{4\pi a_0^2 Z^2 R^2}{m_0^2 c^4} \cdot \frac{1-\beta^2}{\beta^4} \left\{ \frac{E_{max}}{E_{min}} + 2\pi Z\alpha\beta \cdot \left(\frac{E_{max}}{E_{min}}\right)^{1/2} \right.$$
$$\left. - \left[1 + 2\pi Z\alpha\beta + (\beta^2 + \pi Z\alpha\beta) \cdot \ln(\frac{E_{max}}{E_{min}}) \right] \right\} \quad (3)$$

Where, a_0 is the Bohr radius, Z is the atomic number, R is the Rydberg energy, m_0 is the rest mass of the electron, c is the speed of light, β is the electron velocity as a fraction of c ($\beta = \frac{v_e}{c}$), α is the fine structure constant, and E_{min} is the minimal energy required for sputtering. Additionally, E_{max} is the maximum energy that can be transferred from a high energy electron to an atom, and is calculated as is shown in Equation 4.

$$E_{max} = \frac{E_0(E_0 + 2m_0c^2)}{E_0 + \left(1 + \frac{m_0}{M}\right)^2 \frac{Mc^2}{2}} \tag{4}$$

Where E_0 is the energy of an incoming electron and M is the mass of the target nucleus.

The complicating factor of Equation 3 is that the minimal energy to remove an atom, E_{min}, is not necessarily well known. For solid materials values between the sublimation energy, E_{sub}, and twice E_{sub} have been suggested to be appropriate approximations E_{min} [30]. Egerton however suggests that $5/3 \cdot E_{sub}$ models the behavior of metallic solids better than both E_{sub} and $2E_{sub}$ and should be used [29].

Equation 3 implies that there exists, for any material, an energy of incoming electron below which there is no sputtering. However, as is discussed in Paper I, materials are often damaged by the electron beam below this theoretical threshold. To bring up an example from Paper I, graphene exhibits a threshold of $110\,\mathrm{keV}$ [31, 32], however, it has been shown that C will sputter from graphene at $90\,\mathrm{keV}$ and show a smooth increase in sputter rate up to $110\,\mathrm{keV}$ [31]. Additionally, Carbon nanotubes have a theoretical sputtering threshold of $86\,\mathrm{keV}$ but sputtering has been shown to occur at $80\,\mathrm{keV}$ [33]. Both references [31] and [33] provide explanations for this discrepancy; thermal lattice vibrations in parallel with the electron momentum reducing the minimum energy required, and defects in the carbon structure respectively. However, these examples illustrate the complexity of these types of interactions.

Furthermore, solving Equation 3 for TEM–relevant electron energies, there is no major decrease in the sputtering cross–section over the entire energy range, this is illustrated in Figure 2. This is essentially the opposite of the effect seen in the inelastic case as illustrated by Figure 1. As such, changing the electron energy, within a reasonable TEM–relevant range and dependant on the material, is expected to decrease the inelastic effects while the elastic effects either stay constant, decrease slightly or even increase.

1.3   Loss of Oxygen

As per Equation 3, the sputtering cross-section is dependent on the atomic mass; consequently, lighter elements, such as oxygen, are readily ejected from, for example, oxide
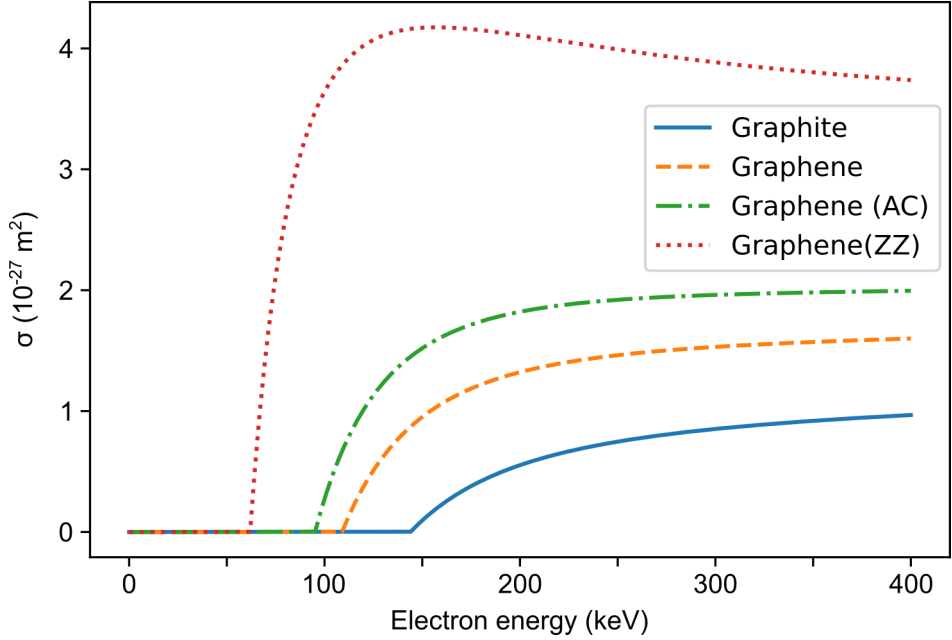
Figure 2: Sputtering cross–section for graphite and graphene. For graphene, both the armchair (AC) and the zig-zag (ZZ) edge–terminations are considered as well as the bulk values. $E_{min} = E_d$ for all calculations, with data sourced from reference [32].

lattices. This can lead to a breakdown of an oxide structure, and lead to general reduction of the oxide. It has been shown that this type of damage is limited in extent to when the sample becomes conductive, and has been shown for both bulk oxides [9] and for thin oxide films [34]. However, both references [9] and [34] note that this effect is likely a combination of radiolysis and knock-on sputtering. Another example is the sputtering of oxygen from a platinum oxide surface layer, which was quickly reduced as the sample was irradiated by high energy electrons. When the sample was not subjected to the electron beam in the TEM, the oxide remained intact [23]. Another type of oxygen–containing material that is sensitive to electron irradiation is clays, which in general consists of silica (SiO_2) and alumina (Al_2O_3). The clay tends to amorphize after short periods of electron irradiation, although there it is likely radiolysis that is the dominant factor [35, 36].

This preferential sputtering of lighter elements results in difficulties in working with samples with light elements, as such extra consideration needs to be taken to ensure that the electron dose rate is low enough to not damage the sample beyond recognition.

2   Emission of low energy electrons

Several interaction processes can result in electrons being ejected from target atoms by high energy electrons. These ejected electrons can be loosely categorized into three categories depending on their kinetic energy. Firstly, electrons can be ejected from the conductance or valence bands of the target material, these possess low energy, and will be referred to as secondary electrons. Higher in energy are electrons ejected from inner shells during relaxation of ionized atoms, which will be referred to as Auger electrons[4]. This generation mechanism results in well–defined possible energies for Auger electrons, which can consequently be used for elemental analysis of the irradiated sample. Auger electrons have energies in the range of a few hundred eV to a few keV. There are also the core–shell electrons knocked away from the target atom and instigating the primary event for both Auger and characteristic X–ray emission, there should be no fundamental difference between these and secondary electrons other than the generation mechanism.

High energy electrons interacting with electrons in the conductance or valence band of a target atom gives rise to the emission of low energy electrons. These resultant electrons are referred to as secondary electron, and generally have energies less than 50 eV, as is illustrated for a few different elements in Figure 3. The emission of secondary electrons from a metal under electron irradiation can be modeled with the framework provided by Chung and Everhart [37].

$$f(E) = \frac{E - E_F - \Phi}{(E - E_F)^4} \tag{5}$$

Where $f(E)$ is the shape of the energy distribution of emitted secondary electrons, and E, E_F, and Φ are the ionization energy, Fermi energy, and work function of the material respectively. Equation 5 does not provide absolute secondary electron yields, only relative yields of different energies. Notably, the emission is fully independent from the energy of the incoming electrons, at least for energies above approximately 100 eV, which is well below the energies used in TEM [37].

A more useful implementation of Equation 5 is that utilized by [38], where the absolute energy of stimulating secondary electron emission is not the desired quantity, rather the energy above the vacuum level E_{vac}, i.e. the energy the electrons will have once they are free from the surface. This is done by setting $E = E_{vac} + E_{SE}$, and noticing that $E_{vac} = E_F + \Phi$, then Equation 5 can be rewritten as,

---

[4]Some authors, notably [14], also refer to these as secondary electrons, however, I have chosen to separate these categories due to the difference in generation and energy spread. However, I do recognize that there are no fundamental differences between the three categories specified here.

$$f(E_{vac} + E_{SE}) = \frac{E_{SE} + E_{vac} - E_{vac}}{(E_{SE} + E_{vac} - E_F)^4}$$

$$= \frac{E_{SE}}{(E_{SE} + E_F + \Phi - E_F)^4} \tag{6}$$

$$= \frac{E_{SE}}{(E_{SE} + \Phi)^4}$$

This is a useful form as it allows for estimation of the shape of Equation 5 with only one material parameter, the work function Φ.
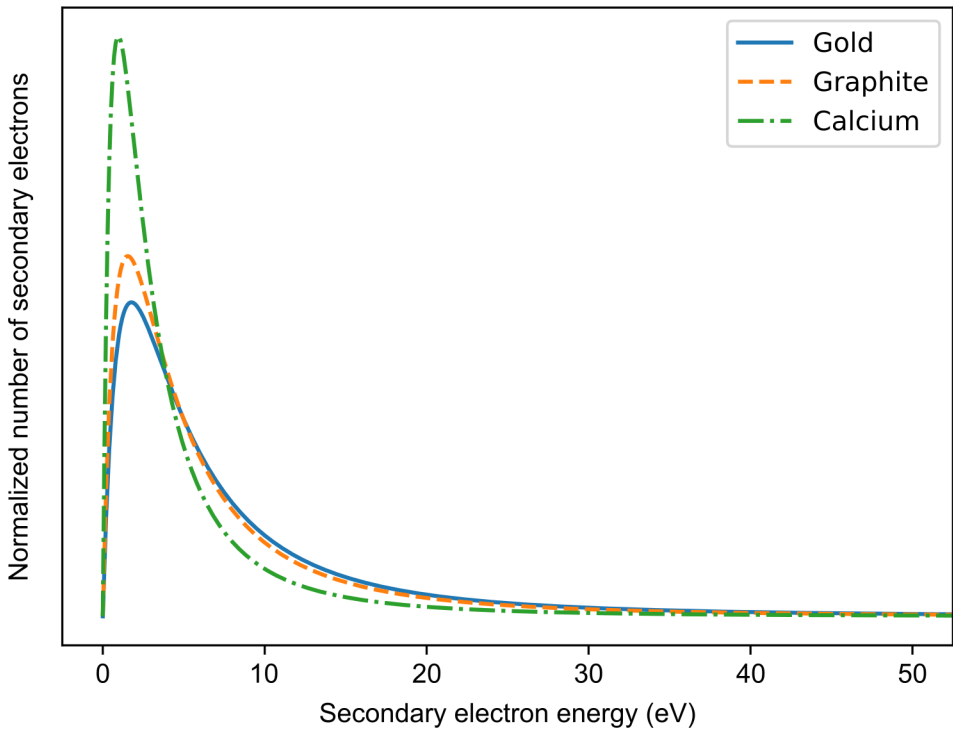
Figure 3: The distribution of secondary electrons emitted from common metals as calculated with Equation 5. $\Phi_{Au} = 5.30\,\text{eV}$ [39], $\Phi_{Graphite} = 4.62\,\text{eV}$ [40], and $\Phi_{K} = 2.87\,\text{eV}$ [41] were chosen to provide a range of different elements with different work functions.

This simple theoretical treatment nevertheless fits well to the experimental data complied by Patino et al. for electrons impacting graphite [38]. However, some electron coincidence spectroscopy studies have shown that this theoretical treatment is perhaps a bit too simplistic, and does not necessarily fit very well to all data [42]. Nonetheless, the important aspect of secondary electrons as a concept is not the absolute energy spread

of the secondary electrons. Rather, it is that the secondary electrons possess a much lower energy than the primary electrons, $100\,\mathrm{eV}$ or less as compared to 80–$300\,\mathrm{keV}$, the implications of which will be discussed in Chapter 4.

If an atom is ionized through the electron impact induced ejection of an inner core–shell electron, the atom is left with a highly unstable electronic configuration. This instability is quickly quenched by an electron in a higher electron–shell losing energy and dropping into the lower energy vacancy. This requires the electron to lose energy, which it can either do as a characteristic X-ray[5] or through Auger emission, where another electron picks up the energy of the electron dropping into the primary ionization hole, and is ejected. The Auger emission is also characteristic in energy, whereas the energy of a characteristic X-ray is related to only the energy difference between the shell from which an electron is ejected and the shell from which the filling electron comes. The energy of an Auger electron depends on the binding energies of the shell of the primary ejection, the shell of the electron losing energy, and shell containing the electron soon to be an Auger electron, binding energy of the shell containing the Auger electron is that for the ionized specie of the atom [43].

2.1 Short note regarding electron energy loss spectroscopy

The act of ionizing a sample to eject secondary electrons of any energies requires an energy transfer from the incoming high energy electron to the bound electrons of the material. Therefore, some of the incoming electrons will have appreciably less energy after passing through the sample as opposed to before. This energy loss can be small, as would be the case of exciting valence electrons (on the order of 10^0–10^1 eV), or large, as would be the case of exciting core–shell electrons (10^2–10^3 eV). If the energy of the electrons that have passed through the sample is measured, the history of the electron can be inferred, albeit with some limitations. Thus providing elemental and chemical information about the sample. This process is called electron energy loss (EEL) spectroscopy and more information regarding it can be found in [44].

---

[5]Characteristic X–rays have an energy characteristic to the energy difference between the two relevant electron energies, and can be used to identify elemental composition. There is a commonly used spectroscopic method based around the emission of characteristic X–rays, Energy dispersive X–ray spectroscopy (which is infuriatingly shortened to either EDX, XEDS, or EDS), whereby a sample is irradiated and the X–rays are collected. Since the energy of the X–rays depends on the energy difference between two core–shells, they are element specific and can be used to determine qualitatively and quantitatively which elements are present in the sample.

Chapter 3: ETEM considerations

In an ETEM, the electrons pass through a gas as well as through the solid sample, which facilitates electron–gas interactions and electron–gas–solid interactions in addition to the electron–solid interactions discussed in Chapter 2. For example, the gas can be ionized and may react with the sample in ways that is not representative of what would occur outside the microscope. Additionally, the sample can be damaged in a way that allows the gas to react with it in non–representative ways. These extra interactions add even more complexity to the issue of electron–sample interactions.

1 Gas–electron interactions

It has been shown that the composition of gas in the ETEM can be determined with both valence and core–shell EEL spectroscopy [45], which indicates that some ionization occurs in the gas phase. However, the extent at which gas molecules are ionized within the ETEM is a largely unexplored topic. As the eponym of this thesis, a discussion of molecular oxygen is warranted.

1.1 Electron interactions with O_2

A useful example that has been quoted as having an impact in oxidation of carbonaceous materials in the TEM is the gas-phase interactions between electrons and oxygen gas. Sediako et al. [46] has presented four chemical reactions that occur in flames that could reasonably also occur in the electron beam.

$$O_2 + e^- \rightarrow O_2^- \qquad\qquad [1]$$

$$O_2 + e^- \rightarrow O_2^+ + 2\,e^- \qquad\qquad [2]$$

$$O_2 + e^- \rightarrow O^+ + O + 2\,e^- \qquad\qquad [3]$$

$$O_2 + e^- \rightarrow 2\,O + e^- \qquad\qquad [4]$$
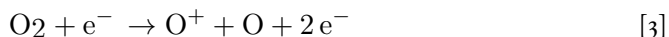
Reactions [1]–[4] show that there are three possibilities for ionization, dissociative electron capture [1], direct ionization [2], and dissociative ionization [3]; pure dissociation [4] will be discussed later. Of these, both direct ionization [2] and dissociative ionization [3] result in positive oxygen species, while dissociative electron capture [1] results in negative oxygen species. These four reactions do not cover the entire space of possible O_2–electron interactions, for example, more than one electron can be ejected during a dissociative ionization, however, the cross–section of this is two orders of magnitude smaller than just one electron being ejected. These four are discussed since they are present in flames [46] and therefore relevant for the observations of high–temperature oxidations, for example of Carbon black as is discussed in Paper I. At TEM relevant energies, electron ejection via [2] and [3] is much more likely than electron capture via [1]. This is illustrated in Figure 4 using data compiled by Itikawa [47] and Equation 2 and the data found in Table 1.
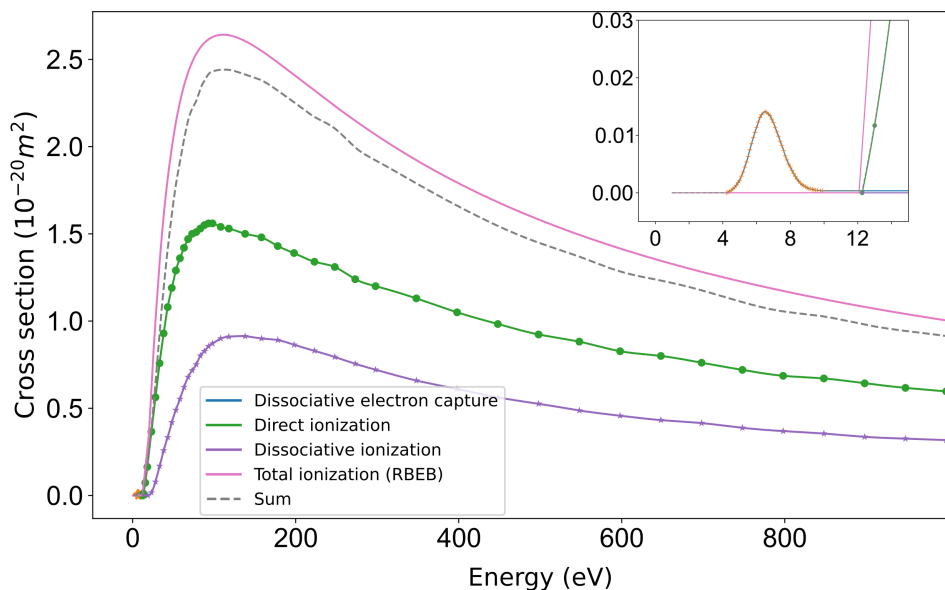
Figure 4: Ionization cross–sections as calculated by Equation 2 for O_2 as compared to data collected by Itikawa. The data for the dissociative ionization (Reaction [3]) and the direct ionization (Reaction [2]) are interpolated with a cubic spline interpolant in order to form a smooth curve for comparison to the RBEB calculations. The inset shows the cross–section for dissociative attachment (Reaction [1]).

The sum of the data for dissociative ionization and direct ionization is consistently less than the cross–section as calculated by RBEB. This is not unexpected as the two main effects considered in Figure 4, direct ionization and dissociative ionization do not cover the full range of possible effects. That is to say, the RBEB model in this case covers more potential interactions than the two listed here. Specifically, the double electron ejection case discussed above, however, it is also possible that RBEB is simply overestimating the

cross–sections. Regardless, ass the RBEB–curve is consistently larger than the sum of Reactions [1], [2], and [3], it can be used as an upper bound of the sum of these Reactions as the electron energy increases. The energy dependence of the RBEB model for O_2 can be found in Table 2. Additionally, from the inset, the cross–section of dissociative attachment is vanishingly small compared to the other two.
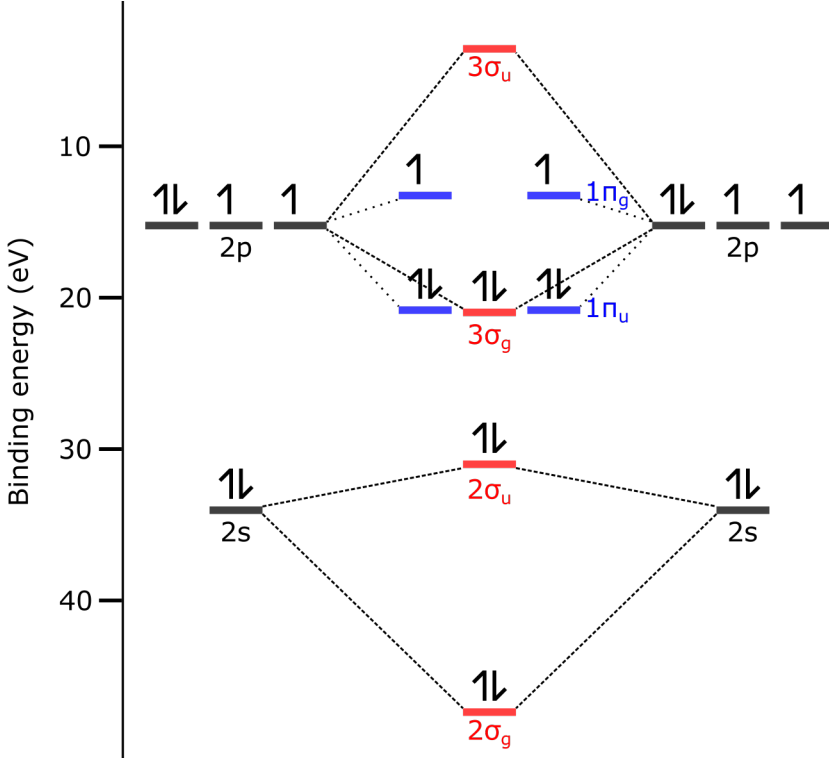
Figure 5: Molecular orbitals of oxygen constructed to scale (disregarding $3\sigma_u$ as the molecular orbital is not occupied) with data from [27] and [48].

Table 1: RBEB values for triplet Oxygen, data from reference [27]. The cross-section values were calculated with Equation 2. For a reminder of which molecular orbital is which, see Figure 5

MO	B (eV)	U (eV)	N	$\sigma_{100\,keV}$ $(10^{-23}\,m^2)$	$\sigma_{300\,keV}$ $(10^{-23}\,m^2)$
$2\sigma_g$	46.19	79.73	2	1.74	0.96
$2\sigma_u$	29.82	90.92	2	2.82	1.55
$1\pi_u$	19.64	59.89	4	8.95	4.88
$3\sigma_g$	19.79	71.84	2	4.44	2.42
$1\pi_g$	12.07	84.88	2	7.62	4.14
Total				25.57	13.39

1.2 Dissociation of O_2

It is tempting to describe Reaction [4] as a sputtering process as it involves removing an atom from what could tentatively be described as a lattice via electron impact. However, using the dissociation energy of O_2, which acts as an analogue to the sublimation energy in a solid, as E_{min} in Equation 3 leads to a delayed onset of the cross–section at $35.3\,\text{keV}$[6]. This result is in clear opposition to the data presented by Itikawa [47], both in peak location and in magnitude of the calculated cross–section. Rather, the dissociation of O_2 likely occurs as a consequence of optically allowed transitions within the molecule, the data is expected have a Bethe asymptote on the form shown in Equation 7 [49].

$$\sigma = a\frac{\ln(b \cdot E/E_c)}{E \cdot E_c} \tag{7}$$

Where a and b are fitting parameters, and E_c essentially fulfills the same function as the binding energy in, for example, 1, and is set to the dissociation energy of O_2, $E_c = 5.012\,\text{eV}$ [50]. It is not a coincidence that there are similarities between Equation 1 and Equation 7, since Bethe theory lies at the heart of both. The main difference between ionization and dissociation being that the impacted electron ends up in an excited state rather than in the vacuum as is the case with ionization. Naturally there is also a relativistic extension to Equation 7, as adapted from [14].

$$\sigma = \left(\frac{a}{\left(\frac{m_0v^2}{2}\right)E_c}\right)\left[\ln\left(\frac{b}{E_c} \cdot \frac{m_0v^2}{2}\right) - \ln(1 - \beta^2) - \beta^2\right] \tag{8}$$

Once again, a and b are the same fitting parameters, $\frac{m_0v^2}{2}$ is the relativistic energy of the electron, where m_0 is the rest mass of the electron, v is the relativistic velocity of the electron. Furthermore, $\beta^2 = 1 - \frac{1}{(1+v)^2}$ in the same way as in Equation 2. As is illustrated in Figure 6, fitting Equation 7 and 8 to the data provided by [47], with the estimated 33% uncertainty of the data included gives a reasonable model fit, especially given that cross–section calculations solely based on Bethe theory tend to be unreliable at lower energies [28]. While the majority of pure dissociation of O_2 is likely the result of excitative interactions, a minority may still be generated through the sputtering process.

---

[6]As can be calculated with Equation 3 using $E_{d,O_2} = 5.012\,\text{eV}$.
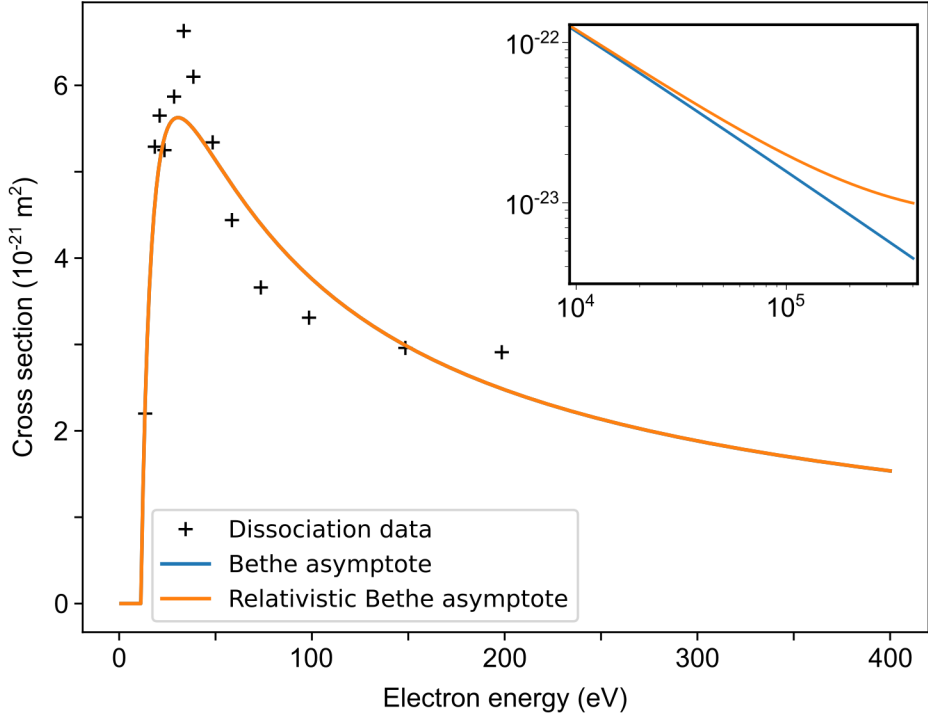
Figure 6: Cross–section of dissociation of O_2 as presented by [47], as well as a model to describe the data based on a relativistic and non–relativistic Bethe asymptote as described in Equation 7 and 8, with $a = 8.62 \times 10^{-19}\,\mathrm{m^2 J^2}$ and $b = 0.44$. The inset shows Equations 7 and 8 extrapolated to high electron energies.

1.3 Impact of ionization in the ETEM

While ionization of O_2 does occur in the ETEM, the fraction of O_2–ions or radicals will be small compared to molecular oxygen under all realistic ETEM conditions. In order to estimate the fraction of ionized species present, we consider the most extreme case, where no ionized species will be neutralized in the sample chamber, but only exit through the differential pumping aperture. The fraction of ionized species (F) will reach a steady state where the rate of formation (through ionization by the beam) and removal through pumping are equal.

$$\frac{dF}{dt} = \frac{\sigma I n_i}{n_{tot}} - F \cdot \frac{\dot{n}}{n_{tot}} \tag{9}$$

Where σ is the cross–section, I is the electron beam dose rate, n_i is the number of O_2 in beam path, n_{tot} is the total number of oxygen atoms in the column, $\dot{n}$ is the flow-rate of O_2 by the mass flow controller, and F is the fraction of ionized oxygen species. This

can be rewritten assuming O_2 is an ideal gas.

$$\frac{dF}{dt} = \sigma I \frac{\frac{pV_I}{k_B T}}{\frac{pV_{tot}}{k_B T}} - F\dot{n} \cdot \frac{k_B T}{pV_{tot}} = \sigma I \cdot \frac{V_I}{V_{tot}} - F\dot{n}\frac{k_B T}{pV_{tot}}$$

Where k_B is Boltzmann's constant, T is the gas temperature, p is the pressure in the chamber, V_I is the volume of the gas in the electron beam path, and V_{tot} is the total volume of gas present in the microscope. If we assume that the volumes are cylindrical, and that there is a constant pressure in the chamber, and only in the chamber, then the length of the chamber and where the beam can interact with oxygen atoms are the same.

$$\frac{dF}{dt} = \sigma I \frac{\pi r_I^2 \cdot l}{\pi r_{tot}^2 \cdot l} - F\dot{n}\frac{k_B T}{pr_{tot}^2 l} = \sigma I \left(\frac{r_I}{r_{tot}}\right)^2 - F\dot{n}\frac{k_B T}{pr_{tot}^2 l} \tag{10}$$

A set of values reasonable for typical experimental conditions are given below.

$$\sigma = 5 \times 10^{-22}\,\mathrm{m}^2 \qquad\qquad I = 10^{24}\,\mathrm{e^- m^{-2} s^{-1}}$$
$$r_I = 100 \times 10^{-9}\,\mathrm{m} \qquad\qquad r_{tot} = 0.5 \times 10^{-2}\,\mathrm{m}$$
$$p = 1\,\mathrm{Pa} \qquad\qquad T = 300\,\mathrm{K}$$
$$l = 10^{-2}\,\mathrm{m} \qquad\qquad \dot{n} = 4.5 \times 10^{17}\,\mathrm{s}^{-1}$$

Then, solving Equation 10 with initial condition $F(0) = 0$, the steady state O_2–ion fraction is on the order of one billionth. Keep in mind that there are many assumptions made during the derivation of both Equations 9 and 10, as such this number should be considered as a guide to an approximate order of magnitude of the ionized fraction. The true steady state number of ionized species is likely smaller as there are more ways that the concentration of ionized species can decrease. The concentration of ionized species will likely decrease due to impacts with the microscope column. However, since secondary electrons have much lower energy than the high energy electrons, the ionization cross–section much larger, so if there is a large generation of secondary electrons, the true steady state may be larger. However, it seems unlikely that the generation of secondary electrons is so large as to counteract the added interaction potential of the ionized species. If the solution to the integrated form of Equation 10 is treated as a guideline to the order of magnitude of ionized species present, the results will likely generalize to many small gas molecules.

1.4 Summary of interactions involving O_2

A summary of the cross–sections relating to O_2 at common electron energies used in TEM can be found in Table 2. As can be seen the largest factor by far is from the ionization reactions indicating that the predominant reactions relating to O_2 are [2] and [3]. However, from Equation 10 the fraction of ionized oxygen species overall will be small.

A confounding factor is the generation of secondary electrons, if the total yield of secondary electrons is small, then the conclusions above stand on their own merit, and there will be few ionized species. However, if the secondary electron yield is large, the situation may change. From Figures 4 and 6 it is clear that interactions between low energy electrons generated as a secondary electron and the gas will be much more prevalent than those between high energy electrons and the gas. While the energy distribution of secondary electrons does not scale with the incoming electron energy, the amount of secondary electrons does. As per Chapter 2, the secondary electron yield scales with the ionization cross–section, as such, increasing electron energy from $100\,\mathrm{keV}$ to $300\,\mathrm{keV}$ approximately halves the probability of generating a secondary electron.

The effect of secondary electrons on dynamic processes in the ETEM is further enhanced by where the secondary electrons are generated. While ionization events by high energy electrons can occur anywhere in the beam path, i.e. mostly far away from the sample, ionization events caused by secondary electrons will occur much closer to the sample due to the relatively large source of secondary electrons the sample represents. For example, it has been shown that the oxidative etching of carbon nanotubes is faster when the sample is located over a SiN_x film (which acts as a large source of secondary electrons) as opposed to over vacuum [51]. Secondary electrons add a secondary effect to lowering the electron energy, not only will the primary electrons interact more with the sample and the gas, but they will also generate more secondary electrons which will further enhance any electron beam observed effects.

Table 2: A summary of the cross–sections of the different interactions. RBEB describes the upper limit of the sum of Reactions [3] and [2]. Relativistic Bethe describes an approximation of Reaction [1] with the experimental data from [47] as a basis. Mott describes the another approximation of Reaction [1] using the Mott framework as presented in Equation 3. Reaction [4] is not considered due to the cross–section already being less than 5×10^{-24} at $10\,\mathrm{eV}$.

Electron Energies	Relativistic Cross–sections $10^{-24}\,\mathrm{m}^2$		
	RBEB	Relativistic Bethe	Mott
80 keV	299	23.2	0.0218
100 keV	256	19.9	0.0212
200 keV	168	13.2	0.0169
300 keV	139	11.0	0.0149

2 Sample–Gas–Electron interactions

In addition to the gas–electon interaction discussed above, there is also the potential for sample–gas–electorn interactions. A description of how such a reaction interaction would occur is that electron irradiation induced altering of the sample allows for an adsorbed gas molecule to react with the altered site. However, it could also be the case that electron irradiation induced a change in the adsorbed gas molecule to allow it to directly interact with the sample.

An example of the second case is electron beam induced deposition (EBID). EBID is a lithography method wherein metal–organic precursor molecules are allowed to adsorb to a substrate surface. This surface is then irradiated by an intense focused electron beam with an energy of between around 1–30 keV. The cracking[7] of precursors in electron beam induced deposition is modeled as an electron–gas–sample effect in which the electrons crack precursors adsorbed to the substrate, which are then free to interact with the surface. Additionally, the electrons interact with the substrate inelastically to produce secondary electrons which then crack the adsorbed precursors [52]. A similar effect has been suggested to play a role in the cracking of precursors in in–situ metal–organic chemical vapor deposition (MOCVD)[8] as observed by preferential nucleation or by induction of stacking defects due to changing reaction conditions by altering the amount of cracked precursors available [24, 53].

An example of the first case is that the electron irradiation induced defects forming in graphite which are then much more likely to interact with O_2 as well as with adsorbed O. These defects would be formed by elastic effects, as such changing the electron energy will change the cross–section in a minor way.

---

[7]Cracking a metal–organic molecule is essentially a process in which the organic molecules are removed from the metal, in this case by electrons causing radiolysis of the bonds, but thermal energy is also commonly used.

[8]I.e. inside an environmental transmission electron microscope.

Chapter 4: Mitigation strategies for beam effects

The electron–solid, electron–gas, and electron–gas–solid interactions discussed in the previous two chapters pose a fundamental challenge for the interpretation of data acquired with electron microscopy. *Are we observing the material as it is or as the electron beam determines it to be?* and *Is the process we are seeing intrinsic or is it in part or fully induced by the electron beam?*

Neither of these questions are trivial, yet their consideration of vital importance for understanding the limitations of the analysis of TEM and ETEM data, and can inform decisions about how these data are acquired.

1   Changing microscope parameters

In order to limit the impact of electron irradiation on materials, some parameters in the electron microscope can be changed. One possibility is to change the illumination parameters, i.e. the electron dose rate and primary electron energy. The interaction rate can be defined as a function of the interaction cross–section, the number of atoms to be interacted with, and the flux of electrons where changing the two parameters leads to different expected changes in the interaction rate. Changing the primary electron energy changes the interaction cross–section non–linearly, leading to a non-linear dependence of the interaction rate to the primary electron energy. The number of atoms is not easily changed, however imaging the sample over vacuum as opposed to over a SiN_x film is one way to do so. A change in the flux of electrons, i.e. the dose rate, will have a clear effect on the interaction rate, the interaction rate should increase with increased dose rate. The effect on the observed rate of interaction seen by changing these two variables is discussed in the following sections.

1.1 Electron dose rate

The simplest method of limiting the effect of electron beam damage is to limit the number of electrons passing through the sample. This is common in cryo-electron microscopy[9], where the total dose is generally limited to less than $100\text{ e}^-\text{Å}^{-2}\text{s}^{-1}$, and less than $10\text{ e}^-\text{Å}^{-2}\text{s}^{-1}$ is not uncommon [55][10]. As an example for how conventional hard material science is conducted, take Paper I where the lowest dose rate used is on the order of $200\text{ e}^-\text{Å}^{-2}\text{s}^{-1}$ and samples are observed at this dose rate for several minutes, leading to a large total dose[11]. However, there are very different goals and challenges relating to the two applications; biological samples are much more beam sensitive than hard materials, and atomic resolution is not necessarily desired. Additionally, for hard materials, ionization is not as important as a damage mechanism as in biological samples.

Electron irradiation damage is not instantly observable in samples, rather samples need to be exposed to electrons for a time before they are damaged[12], this concept is known as a characteristic dose [56]. However, some studies show that electron irradiation damage in hard materials tends to be more dependent on dose rate rather than total dose [56, 57]. That there would exist a lowest dose/dose-rate where no noticeable electron beam damage occurs gives rise to a definition of a threshold dose/dose-rate. There is some debate whether dose rate, total dose, or both dose rate and total dose are important to limit when limiting irradiation damage. Both Jiang et al. [56] and Kisielowski et al. [57] show that hard materials tend to be more sensitive to the dose rate and attribute this to a damage relaxation mechanism whereby bonds break rapidly but reform faster than atoms can be removed. However, as the dose rate is further increased, the relaxation may not be enough to compensate for the amount of irradiation induced damage. For soft matter, there are results showing no dependence on the dose rate, but rather on the total dose [11]. However, these differences may be due to the minuscule energy threshold dose for damage to be realized for organic samples due to the predominant damage type being radiolysis. For hard materials, the predominant damage type is knock-on effects with a larger energy threshold for inorganic samples [58]. As such, it may be that inorganic samples are more able to relax knock–on damage than organic samples are to relax radiolysis–induced damage. Since this thesis mainly deals with inorganic material, a threshold dose rate will hereafter be referred to, and a threshold total dose will remain untreated. Nevertheless, as is seen from the biological applications of TEM,

---

[9]Cryo–electron microscopy involves cooling of the sample to liquid nitrogen temperatures in order to reduce beam damage caused, as well to immobilize biological components for imaging. For further reading, see [54].

[10]Note that the dose for cryo–EM is often provided as a total dose ($\text{e}^-\text{Å}^{-2}\text{s}^{-1}$), not a dose rate ($\text{e}^-\text{Å}^{-2}\text{s}^{-1}$) as is done in Paper I, and in discussions of hard-materials in general

[11]For comparison with Paper I: $1\text{ e}^-\text{Å}^{-2}\text{s}^{-1} = 100\text{ e}^-\text{nm}^{-2}$. In other words

[12]Or damaged enough for the damage to be detectable in the TEM.

one solution for limiting both these damage mechanisms is to reduce the number of electrons. However, this will limit the signal–to–noise ratio, which limits the amount of useful data that can be collected.

In dynamic processes

In dynamic processes the response to dose rate is not as simple as in the static case, there are many other effects involved, and the sample is, by definition already being probed. The primary example being the presence of more potential interactions samples are observed under a gas pressure. In order to determine the dose rate dependence of a reaction can be done by observing the reaction at a series of different dose rates and extrapolating the effect to a dose of 0. This is discussed in Paper I, where the dose rate dependence of carbon black oxidation is found to be non-linear as the increase of the oxidation rate diminishes as the dose rate increases. Figure 7 shows that the oxidation rate, denoted as radius decrease, begins by increasing rapidly as the dose rate increases; but with further increases to dose rate, the oxidation rate increases less signifying a saturation of the electron beam induced oxidation rate. This effect is observed both at a low pressure of $1\,\mathrm{Pa}$ (B) and at higher pressure of $1500\,\mathrm{Pa}$ (A), which rules out a saturation of ionized species in the gas.

In (B) the radius reduction is compared against what is referred to as a 0–dose measurement in Paper I, this is the green zone and represents an oxidation rate when the only electron irradiation occurs during short periods when snapshot images of the material were acquired. This leads to another definition of a potential threshold dose rate, whereby it is defined as when the inherent process is no longer more prevalent than the effect of the electron beam. This definition is of course only applicable when probing the sample with some stimulus other than the electron beam, for example subjecting the sample to oxygen and heating. As an example of this definitions potential usage, in Figure 7 the electron dose rates 1–5, contain data points within the 0–dose region, and could therefore be considered to not be above the threshold dose rate. However, really only 1–2 have a majority of their data points within the 0–dose region, and may so be defined as being below the threshold. Depending on the interpretation of more prevalent used in the definition, 3–4 may also be included as being below the threshold as their means are smaller than twice the maximum value of the 0–dose region, indicating that the intrinsic effects are still the majority of the observed interaction.

This definition of the threshold dose rate provides ground for useful discussion regarding the choice of microscopy parameters when conducting this type of experiment. From the data presented in Paper I, the dose rate should be kept below at most $10^5\ \mathrm{e^-\,nm^{-2}\,s^{-1}}$ to keep the electron beam induced effects from dominating the total reaction rate. However, even lower dose rates is likely better, although one then has to consider the trade–off between electron beam damage and a reasonable signal–to–noise ratio.

1.2 Primary Electron energy

Another possibility of reducing the interaction rate is to change the primary electron energy. Both ionization (Equation 2) and knock-on (Equation3) are dependent on the primary electron energy. In Equation 2, when the primary electron energy (T) changes, both β_t^2, t, and t' change due to their direct relationship with T. For Equation 3, both β and E_{max} change when changing T. A summary of the effects of changing T can be found in Table 2 in Chapter 3.

From Table 2, it is clear that increasing the primary electron energy will decrease the ionization cross–section, and therefore the ionization rate should decrease, given that the dose rate and number of atoms is constant. However, as per Figure 2, some materials have not yet reached their maxima at TEM relevant electron energies, as such the sputtering cross–section can increase with increasing primary electron energy. As an example, for the oxidation of carbon black, if we assume that the material is similar to other carbon nanostructures, the sputtering cross–section will have a energy threshold below which sputtering should not occur. However, in experimental data, there are confounding factors. First of all, back in Chapter 2, the influence of the nanostructure of the material was alluded to, whereby carbon nanotubes experienced sputtering because of defects in its structure. This is a general phenomenon in carbon, the cross–section of sputtering increases around defects in graphite [59]. In the dynamic case of graphite oxidation, this functionality of increased cross–section around defects will become a bit of a feedback loop as defects are more sensitive to oxidation, and will thus oxidize faster and create a further defect. This primarily introduces difficulties into the interpretation of the concept of an energy threshold introduced in Equation 4, and Figure 2. Purely from Figure 2, if the electron energy is reduced to 100 keV, neither graphite nor bulk graphene should experience knock–on damage, however it has been shown that graphene will appreciably lose atoms to knock–on damage at 90 keV [31].

The result of this is again illustrated in Figure 7 where the dependence of the oxidation rate of carbon black on dose rate is plotted for two different cases. From Figure 7, it is clear that if there is a difference in the oxidation rate between the high electron energy (300 keV) and the low electron energy (80 keV or 100 keV); then the oxidation rate is higher for the high energy with the same dose rate. This is counter to what is expected from Table 2. From this, there seems to not be a clear answer to how to limit the effect of the electron irradiation by changing the primary electron energy. However, an effect that was found to be applicable to the setup used when collecting data for Paper I was that the contrast in micrographs increased for 100 keV electrons, as such less of them were needed. Therefore using the lower voltage may result in a smaller effect due to fewer electrons being required to form images without a noticable loss of quality, which is in agreement with the conclusions from reference [60].
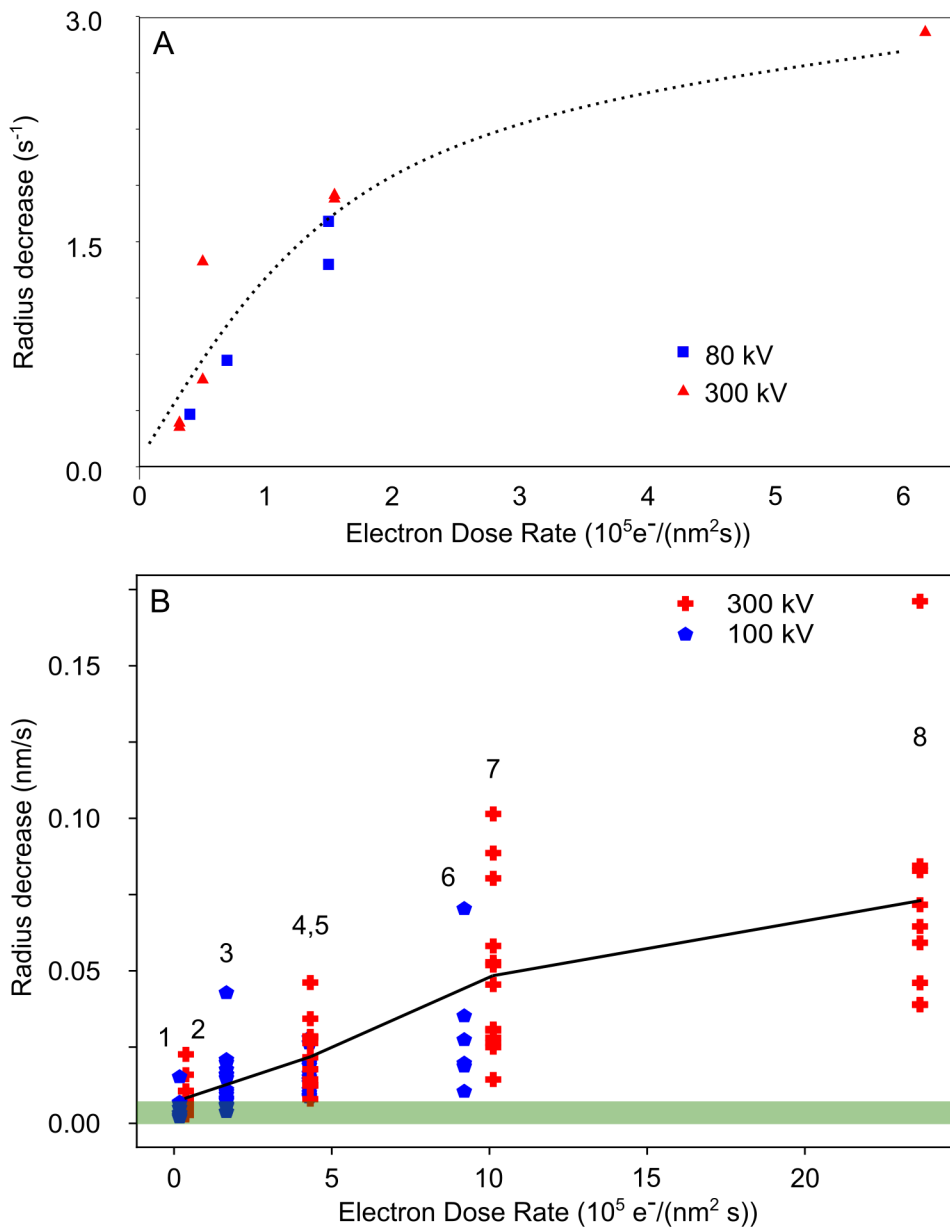
Figure 7: The oxidation rate of Carbon Black at $600\,^{\circ}\mathrm{C}$, displayed as a radius decrease rate. (A) displays the EEL signal reduction rate in the high pressure ($1500\,\mathrm{Pa}$ O_2) data. The dotted line is a guide for the eye to better illustrate the saturation effects at higher dose rates. (B) displays the absolute radius decrease of individual particles observed at $1\,\mathrm{Pa}$ O_2. Here the black line connects the mean of each $300\,\mathrm{keV}$ data point, the green zone represents the oxidation as it occurs with low electron irradiation, as measured by taking occasional snapshots at low magnification and dose. Dose rates 4 and 5 overlap, 4 is the dose rate for $100\,\mathrm{keV}$ and 5 is the dose rate for $300\,\mathrm{keV}$. Reproduced, with modification, from Paper I.

2 Using gases to mitigate electron irradiation effects

The introduction of gases into the TEM introduces additional potential beam interactions as per Chapter 3, but it also supplies additional methods for limiting or counteracting some effects of electron beam irradiation.

While collecting data for Paper II we found that Co–Ni nanoparticles underwent rapid oxidation when irradiated by the electron beam. This is unexpected, the electron beam is expected to have a reducing effect by preferentially knocking out oxygen atoms. Residual gas analysis of the gas–outflow line of the microscope detected no O_2 but did detect H_2O. It is well known that the electron beam can split physiosorbed water molecules into Hydrogen and hydroxide groups. The hydroxide will then chemisorb to the metal, forming a hydroxide. This hydroxide may be further oxidized via ejection of the hydrogen, either through electron beam sputtering or via reactions with other physiosorbed hydrogen atoms. This may be the effect that was observed when the particles are viewed in the background vacuum of the TEM.

Various density functional theory calculations show that water will readily dissociatively adsorb on Ni {111}, {110}, and {100} surfaces forming chemisorbed H and OH, which can further dissociate into H and O [61]. Furthermore, the dissociation is enhanced at steps in the surface, but can be hindered by dopants at higher coverages [62]. Co surfaces also facilitate dissociative adsorption of water on {0001} surfaces at low coverages, with the material forming a passivating oxide layer at higher coverage [63]. Additionally, both Co_3O_4 [64] and NiO [65] surfaces can also cause dissociative adsorption of water. Both the pure bimetallic particles and their corresponding oxides are therefore likely to have chemisorbed oxygen on their surface.

If electron beam induced splitting of physiosorbed water molecules was occurring, two potential mitigation strategies present themselves. Firstly, remove any water from the microscope column[13], or secondly, introduce the sample to a reducing atmosphere. In regular TEM, a cold trap is often used to give volatile components a large, cold surface to deposit on. Employing a cold trap reduces the effect, however, not enough to allow for prolonged exposure, as is shown in Table 3.

---

[13]In gas phase of course, I was once told at a conference about a microscope where by the way of a leaky lens–cooling system the microscope slowly filled with water. This was not the case here.

Table 3: Atomic percent of O, Co, and Ni from before and after a set time of electron irradiation, with and without $0.5\,\mathrm{Pa}$ H$_2$. The measurements are in atomic-% as given by Aztec when only considering O, Co, and Ni. All measurements were conducted with a cold trap present.

Time	Without H$_2$			With H$_2$		
	O	Co	Ni	O	Co	Ni
Start	54.13	30.21	15.67	27.27	48.50	24.23
After 5 minutes	63.38	23.99	12.63	23.45	51.29	25.26
After 10 minutes	–	–	–	29.90	47.89	22.21

As per the EDX data presented in Table 3, introducing hydrogen into the microscope seems to limit the oxidation of the material to a large extent. After harsh illumination of the CoNi for five minutes, without hydrogen the relative oxygen content increases from 1.7 O/Co to 2.6 O/Co while the relative Co/Ni ratio remains constant at 1.9. When introducing hydrogen however, the oxygen content remains at a low[14] 0.6 O/Co. This indicates that the oxidation is greatly reduced when H$_2$ is introduced into the column, and there is no net reduction of the metal oxide, which could allow for imaging of oxides likely to further oxidize or reduce. Therefore, for materials which are sensitive to oxidation from, for example water species, it may be a good idea to observe them under a mild hydrogen pressure.

Another potential gas to be used to limit the effects of electron irradiation damage is O$_2$. As discussed in Chapter 2, oxides are likely to lose oxygen atoms via a combination of radiolysis and knock–on damage. This may be counteracted by the addition of small amounts of O$_2$ to the sample, which could re–oxidize the sample.

---

[14]The oxygen content also starts lower, this is likely due to previous electron beam irradiation of the material.

Chapter 5: Conclusions and Future work

1 Electron–matter interactions are complex

Electron–matter interactions are complex and non–trivial, however their understanding is vital for correct interpretation of TEM data. They must especially be considered during dynamic processes, where there are more vectors whereby electron irradiation damage can influence the results observed. This is exemplified by the findings of Paper I. The interactions between high energy electrons, O_2, and carbon black during oxidation of carbon black are complex, leading to a non–linear response to changes to dose rates. Additionally, the response to changing the primary electron energy is small, which is unexpected as the cross–sections change by a factor of two for inelastic effects. Taking this into account, it is found that the primary mechanism of electron–sample–gas interaction is a knock-on effect. However, this assumes that the energy threshold of the elastic effects can be reduced so much that the lower energies used can cause displacement damage.

Another example that illustrates the importance of considering electron beam effects is that CoNi nanoparticles tend to surface oxidize under electron irradiation, which runs counter to the common understanding that the electron beam has a reducing effect on the material being observed. This effect could be limited by the introduction of H_2 to the sample, however, the present oxides were not re-reduced by the hydrogen.

Essentially, the results from both of these investigations can lead to incorrect conclusions if electron irradiation effects are not considered. The oxide could be considered to be native, or that there is just a loss of crystallinity and that the CoNi is just amorphizing. The influence of high energy electrons in carbon black oxidation may be considered to only influence the O_2, which runs counter to both theoretical, and now experimental data. Electron beam interactions are extremely important for ETEM observations and cannot be ignored.

2   Future Work

A further investigation into the oxidation mechanism of carbon black under electron irradiation is warranted. The EEL spectroscopy sections of Paper I focuses primarily on quantification of the change of the carbon content during oxidation. As such, quite a large dispersion was used in order to include not only the $C-K$ edge but also the $N-K$ and $O-K$ edge, which were included in order to attempt atomic quantification, which was ultimately left as potential future work. However, the large energy range necessary to capture all three of these elemental edges limits the energy resolution around the $C-K$ edge, which limits the possibilities of precise mechanistic interpretations of the EEL data. Therefore, in order to acquire a more mechanistic understanding of the oxidation process of carbon black, more high resolution EEL spectra should be acquired around the $C-K$ edge.

Since the implications of the findings surrounding Paper II were incidental to the actual content of the paper, a more in depth investigation into both the mechanism behind the surface oxidation seen in Paper II and it's origin is warranted. This could potentially give interesting insights into the initiation of oxidation in CoNi, and other oxidation–sensitive materials.

References

[1] Sumio Iijima and Toshinari Ichihashi. Single-shell carbon nanotubes of 1-nm diameter. *Nature 1993 363:6430*, 363:603–605, 1993.

[2] P. Caroff, K. A. Dick, J. Johansson, M. E. Messing, K. Deppert, and L. Samuelson. Controlled polytypic and twin-plane superlattices in iii–v nanowires. *Nature Nanotechnology 2009 4:1*, 4:50–55, 11 2008.

[3] William D. Pyrz and Douglas J. Buttrey. Particle size determination using tem: A discussion of image acquisition and analysis for the novice microscopist. *Langmuir*, 24:11350–11360, 10 2008.

[4] Pau Ternero, Mehran Sedrpooshan, David Wahlqvist, Bengt O. Meuller, Martin Ek, Julia Maria Hübner, Rasmus Westerström, and Maria E. Messing. Effect of the carrier gas on the structure and composition of co–ni bimetallic nanoparticles generated by spark ablation. *Journal of Aerosol Science*, 170:106146, 5 2023.

[5] Marc Adrian, Jacques Dubochet, Jean Lepault, and Alasdair W. McDowall. Cryo-electron microscopy of viruses. *Nature 1984 308:5954*, 308:32–36, 1984.

[6] Rafael Fernandez-Leiro and Sjors H.W. Scheres. Unravelling biological macromolecules with cryo-electron microscopy. *Nature 2016 537:7620*, 537:339–346, 9 2016.

[7] Daniel Wrapp, Nianshuang Wang, Kizzmekia S Corbett, Jory A Goldsmith, Ching-Lin Hsieh, Olubukola Abiona, Barney S Graham, and Jason S Mclellan. Cryo-em structure of the 2019-ncov spike in the prefusion conformation. *Science*, 367:1260–1263, 2020.

[8] Nan Jiang. Electron beam damage in oxides: a review. *Reports on Progress in Physics*, 79:016501, 12 2015.

[9] M. R. McCartney and David J. Smith. Epitaxial relationships in electron-stimulated desorption processes at transition metal oxide surfaces. *Surface Science*, 221:214–232, 10 1989.

[10] Florian Banhart. Irradiation effects in carbon nanostructures. *Reports on Progress in Physics*, 62:1181–1221, 8 1999. See notebook, seminal review on carbon based particles in electron beam.

[11] Zino J.W.A. Leijten, Arthur D.A. Keizer, Gijsbertus De With, and Heiner Friedrich. Quantitative analysis of electron beam damage in organic thin films. *Journal of Physical Chemistry C*, 121:10552–10561, 5 2017.

[12] P G Lucasson and R M Walker. Production and recovery of electron-induced radiation damage in a number of metals. *Physical Review*, 127, 1962.

[13] R. F. Egerton, P. Li, and M. Malac. Radiation damage in the tem and sem. *Micron*, 35:399–409, 8 2004.

[14] David B Williams and C Barry Carter. *Transmission Electron Microscopy: A Textbook for Materials Science*. Springer Science, 2nd edition, 2009. ISBN 978-0-387-76502-0.

[15] R.F. Egerton. *Physical Principles of Electron Microscopy*. Springer International Publishing, 2 edition, 2016. ISBN 978-3-319-39876-1.

[16] Jan-Olov Bovin and Lars Stenberg. *Högupplösande Elektronmikroskopi*. Wallin och Dalholm Boktryckeri AB, 1981. ISBN 91-7422-003-9.

[17] Crispin Hetherington, Daniel Jacobsson, Kimberly A Dick, and Reine Wallenberg. In situ metal-organic chemical vapour deposition growth of iii–v semiconductor nanowires in the lund environmental transmission electron microscope. *Semicond. Sci. Technol*, 35:34004, 2020.

[18] T. W. Hansen, J. B. Wagner, and R. E. Dunin-Borkowski. Aberration corrected and monochromated environmental transmission electron microscopy: challenges and prospects for materials science. *Materials Science and Technology*, 26:1338–1344, 2010.

[19] S. B. Simonsen, S. Dahl, E. Johnson, and S. Helveg. Ceria-catalyzed soot oxidation studied by environmental transmission electron microscopy. *Journal of Catalysis*, 255:1–5, 4 2008. Discusses among other things, the lowest temperature feasable for oxidation. Has great control over electron beam exposure.

[20] Ofentse A. Makgae, Filip Lenrick, Volodymyr Bushlya, Jon M. Andersson, Rachid M'Saoubi, and Martin Ek. Visualising microstructural dynamics of titanium aluminium nitride coatings under variable-temperature oxidation. *Applied Surface Science*, 618:156625, 5 2023.

[21] Peter A. Crozier, Ruigang Wang, and Renu Sharma. In situ environmental tem studies of dynamic changes in cerium-based oxides nanoparticles during redox processes. *Ultramicroscopy*, 108:1432–1440, 10 2008.

[22] Q. Jeangros, T. W. Hansen, J. B. Wagner, C. D. Damsgaard, R. E. Dunin-Borkowski, C. Hébert, J. Van Herle, and A. Hessler-Wyser. Reduction of nickel oxide particles by hydrogen studied in an environmental tem. *Journal of Materials Science*, 48:2893–2907, 4 2013.

[23] Hideto Yoshida, Hiroki Omote, and Seiji Takeda. Oxidation and reduction processes of platinum nanoparticles observed at the atomic scale by environmental transmission electron microscopy. *Nanoscale*, 6:13113–13118, 10 2014.

[24] Marcus Tornberg, Carina B. Maliakkal, Daniel Jacobsson, Reine Wallenberg, and Kimberly A. Dick. Enabling in situ studies of metal-organic chemical vapor deposition in a transmission electron microscope. *Microscopy and Microanalysis*, 28: 1484–1492, 10 2022.

[25] Robin Sjökvist, Marcus Tornberg, Mikelis Marnauza, Daniel Jacobsson, and Kimberly A. Dick. Observation of the multilayer growth mode in ternary ingaas nanowires. *ACS Nanoscience Au*, 2:539–548, 12 2022.

[26] Yong Ki Kim and M. Eugene Rudd. Binary-encounter-dipole model for electron-impact ionization. *Physical Review A*, 50:3954, 11 1994.

[27] W. Hwang, Y. K. Kim, and M. E. Rudd. New model for electron⊠impact ionization cross sections of molecules. *The Journal of Chemical Physics*, 104:2956, 8 1998.

[28] Yong Ki Kim, José Paulo Santos, and Fernando Parente. Extension of the binary-encounter-dipole model to relativistic incident electrons. *Physical Review A*, 62: 052710, 10 2000.

[29] R.F. Egerton, R. McLeod, F. Wang, and M. Malac. Basic questions related to electron-induced sputtering in the tem. *Ultramicroscopy*, 110:991–997, 7 2010.

[30] C. R. Bradley and N. J. Zaluzec. Atomic sputtering in the analytical electron microscope. *Ultramicroscopy*, 28:335–338, 4 1989.

[31] Jannik C. Meyer, Franz Eder, Simon Kurasch, Viera Skakalova, Jani Kotakoski, Hye Jin Park, Siegmar Roth, Andrey Chuvilin, Sören Eyhusen, Gerd Benner, Arkady V. Krasheninnikov, and Ute Kaiser. Accurate measurement of electron beam induced displacement cross sections for single-layer graphene. *Physical Review Letters*, 108, 5 2012.

[32] Andrew Merrill, Cory D. Cress, Jamie E. Rossi, Nathanael D. Cox, and Brian J. Landi. Threshold displacement energies in graphene and single-walled carbon nanotubes. *Physical Review B - Condensed Matter and Materials Physics*, 92:075404, 8 2015.

[33] Ai Leen Koh, Emily Gidcumb, Otto Zhou, and Robert Sinclair. Oxidation of carbon nanotubes in an ionizing environment. *Nano Letters*, 16:856–863, 2 2016.

[34] Krishna Kanth Neelisetty, Xiaoke Mu, Sebastian Gutsch, Alexander Vahl, Alan Molinari, Falk Von Seggern, Mirko Hansen, Torsten Scherer, Margit Zacharias, Lorenz Kienle, V. S.Kiran Chakravadhanula, and Christian Kübel. Electron beam effects on oxide thin films—structure and electrical property correlations. *Microscopy and Microanalysis*, 25:592–600, 2019.

[35] Chi Ma, J. D. FitzGerald, R. A. Eggleton, and D. J. Llewellyn. Analytical electron microscopy in clays and other phyllosilicates: loss of elements from a 9-nm stationary beam of 300-kev electrons. *Clays and Clay Minerals*, 46:301–316, 6 1998.

[36] Th Allard and G. Calas. Radiation effects on clay mineral properties. *Applied Clay Science*, 43:143–149, 2 2009.

[37] M S Chung and T E Everhart. Simple calculation of energy distribution of low-energy secondary electrons emitted from metals under electron bombardment. *Journal of Applied Physics*, 45:707, 1974.

[38] M. I. Patino, Y. Raitses, B. E. Koel, and R. E. Wirz. Analysis of secondary electron emission for conducting materials using 4-grid leed/aes optics. *Journal of Physics D: Applied Physics*, 48:195204, 4 2015.

[39] W. M.H. Sachtler, G. J.H. Dorgelo, and A. A. Holscher. The work function of gold. *Surface Science*, 5:221–229, 10 1966.

[40] S.C. Jain and Kariamanikkam Srinivasa Krishnan. The thermionic constants of metals and semi-conductors i. graphite. *Proceedings of the Royal Society of London. Series A. Mathematical and Physical Sciences*, 213:143–157, 6 1952.

[41] Herbert B. Michaelson. The work function of the elements and its periodicity. *Journal of Applied Physics*, 48:4729, 8 2008.

[42] Alessandra Bellissimo, Gian Marco Pierantozzi, Alessandro Ruocco, Giovanni Stefani, Olga Yu Ridzel, Vytautas Astašauskas, Wolfgang S.M. Werner, and Mauro Taborelli. Secondary electron generation mechanisms in carbon allotropes at low impact electron energies. *Journal of Electron Spectroscopy and Related Phenomena*, 241:146883, 5 2020.

[43] Wolfgang E.S. Unger, Thomas Wirth, and Vasile-Dan Hodoroaba. Auger electron spectroscopy, 9 2020.

[44] R.F. Egerton. *Electron Energy-Loss Spectroscopy in the Electron Microscope*. Springer US, 2011. ISBN 978-1-4419-9582-7.

[45] Peter A. Crozier and Santhosh Chenna. In situ analysis of gas composition by electron energy-loss spectroscopy for environmental transmission electron microscopy. *Ultramicroscopy*, 111:177–185, 2 2011.

[46] Anton D. Sediako, Charles Soong, Jane Y. Howe, Mohammad Reza Kholghy, and Murray J. Thomson. Real-time observation of soot aggregate oxidation in an environmental transmission electron microscope. *Proceedings of the Combustion Institute*, 36:841–851, 1 2017. .

[47] Yukikazu Itikawa. Cross sections for electron collisions with oxygen molecules. *J. Phys. Chem. Ref. Data*, 38, 2009.

[48] Yong-Ki Kim and Jean-Paul Desclaux. Ionization of carbon, nitrogen, and oxygen by electron impact. *Physical Review A*, 66, 2002.

[49] Y. Itikawa, A. Ichimura, K. Onda, K. Sakimoto, K. Takayanagi, Y. Hatano, M. Hayashi, H. Nishimura, and S. Tsurubuchi. Cross sections for collisions of electrons and photons with oxygen molecules. *Journal of Physical and Chemical Reference Data*, 18:23, 10 1989.

[50] Peter Atkins, Loretta Jones, and Leroy Laverman. *Chemical Principles: The Quest for Insight*. W.H. Freeman and Company, 6 edition, 2013. ISBN 978-1-4641-2467-9.

[51] Hideto Yoshida, Yuto Tomita, Kentaro Soma, and Seiji Takeda. Electron beam induced etching of carbon nanotubes enhanced by secondary electrons in oxygen. *Nanotechnology*, 28:195301, 4 2017.

[52] Cornelis W Hagen, W F Van Dorp, and C W Hagen. A critical literature review of focused electron beam induced deposition. *Article in Journal of Applied Physics*, 104, 2008.

[53] Mikelis Marnauza, Marcus Tornberg, Erik K. Mårtensson, Daniel Jacobsson, and Kimberly A. Dick. In situ observations of size effects in gaas nanowire growth. *Nanoscale Horizons*, 8:291–296, 1 2023.

[54] Jacqueline L. S. Milne, Mario J. Borgnia, Alberto Bartesaghi, Erin E. H. Tran, Lesley A. Earl, David M. Schauder, Jeffrey Lengyel, Jason Pierson, Ardan Patwardhan, and Sriram Subramaniam. Cryo-electron microscopy - a primer for the non-microscopist. *FEBS Journal*, 280:28–45, 1 2013.

[55] Koji Kato, Naoyuki Miyazaki, Tasuku Hamaguchi, Yoshiki Nakajima, Fusamichi Akita, Koji Yonekura, and Jian Ren Shen. High-resolution cryo-em structure of photosystem ii reveals damage from high-dose electron beams. *Communications Biology 2021 4:1*, 4:1–11, 3 2021.

[56] Nan Jiang and John C.H. Spence. On the dose-rate threshold of beam damage in tem. *Ultramicroscopy*, 113:77–82, 2 2012.

[57] Christian Kisielowski, Lin-Wang Wang, Petra Specht, Hector A. Calderon, Bastian Barton, Bin Jiang, Joo H. Kang, and Robert Cieslinski. Real-time sub-Ångstrom imaging of reversible and irreversible conformations in rhodium catalysts and graphene. *Physical Review B*, 88:024305, 7 2013.

[58] R. F. Egerton. Mechanisms of radiation damage in beam-sensitive specimens, for tem accelerating voltages between 10 and 300 kv. *Microscopy Research and Technique*, 75:1550–1556, 11 2012.

[59] Chuncheng Gong, Alex W. Robertson, Kuang He, Gun Do Lee, Euijoon Yoon, Christopher S. Allen, Angus I. Kirkland, and Jamie H. Warner. Thermally induced dynamics of dislocations in graphene at atomic resolution. *ACS Nano*, 9:10066–10075, 10 2015.

[60] Mathew J. Peet, Richard Henderson, and Christopher J. Russo. The energy dependence of contrast and damage in electron cryomicroscopy of biological molecules. *Ultramicroscopy*, 203:125, 8 2019.

[61] Abas Mohsenzadeh, Kim Bolton, and Tobias Richards. Dft study of the adsorption and dissociation of water on ni(111), ni(110) and ni(100) surfaces. *Surface Science*, 627:1–10, 9 2014.

[62] Yucheng Huang, Chongyi Ling, Meng Jin, Jinyan Du, Tao Zhou, and Sufang Wang. Water adsorption and dissociation on ni surface: Effects of steps, dopants, coverage and self-aggregation. *Physical Chemistry Chemical Physics*, 15:17804, 10 2013.

[63] Lingshun Xu, Yunsheng Ma, Yulin Zhang, Bohao Chen, Zongfang Wu, Zhiquan Jiang, and Weixin Huang. Water adsorption on a co(0001) surface. *The Journal of Physical Chemistry C*, 114:17023–17029, 10 2010.

[64] Jia Chen and Annabella Selloni. Water adsorption and oxidation at the co$_3$o$_4$(110) surface. *The Journal of Physical Chemistry Letters*, 3:2808–2814, 10 2012.

[65] Wei Zhao, Michal Bajdich, Spencer Carey, Aleksandra Vojvodic, Jens K. Nørskov, and Charles T. Campbell. Water dissociative adsorption on nio(111): Energetics and structure of the hydroxylated surface. *ACS Catalysis*, 6:7377–7384, 11 2016.

Part II

Scientific publications

Author contributions and summary of papers

Paper I: Impact of electron beam irradiation on Carbon Black oxidation in the ETEM

I performed the primary data acquisition, data analysis and manuscript writing.

Summary

Paper I observed the oxidation of Carbon Black in the Environmental TEM under varying dose conditions in order to elucidate the mechanism of the electron–gas–solid interaction resulting in an increase in oxidation rate during electron irradiation. Utilizing both high pressure data (300 Pa) and low pressure data (1 Pa), we concluded that the primary mechanism increasing the oxidation rate is a knock–on effect where atoms are knocked out of position causing reactive sites to appear. Furthermore, ionization of the oxidative gas by secondary electrons close to the sample surface is also determined to have an effect on the increased rate of oxidation. However, ionization of the gas by primary electrons is considered to be unlikely from the data presented in Paper I.

Paper II: Effect of the carrier gas on the structure and composition of Co–Ni bimetallic nanoparticles generated by spark ablation

I performed some TEM data collection, the data-analysis relating to the polycrystalline electron diffraction patterns, and had discussions about this with the main author.

Summary

Paper II discusses the morphological and crystallographic changes in CoNi, and oxides thereof, when modifying the carrier gas from a reducing atmosphere(N_2/H_2) to a slightly oxidative atmosphere (N_2) to a very oxidative atmosphere (Air, i.e. N_2/O_2). The primary findings are that agglomerates of particles generated with N_2/H_2 and N_2 tend to be chains, whereas those produced with Air are produced as individual particles. Additionally, the Co/Ni ratio is constant over all three production parameters, however, both the N_2 and Air produced particles show oxidization, the Air produced particles were fully oxidized and the N_2 mostly contained oxides of Co. Important for this thesis is the collection of TEM and ETEM data not necessarily used within the publication, herein was found that the CoNi particles quickly oxidized under the electron beam, likely due to adsorbed water or oxygen.

LUND

UNIVERSITY

Department of Chemistry
Faculty of Engineering

9 789174 229547